Journal of Building Engineering 54 (2022) 104611

Contents lists available at ScienceDirect

Journal of Building Engineering

journal homepage: www.elsevier.com/locate/jobe

Deformational behavior of self-compacting concrete containing recycled aggregate, slag cement and green powders under compression and bending: Description and prediction adjustment

Víctor Revilla-Cuesta [a,*], Vanesa Ortega-López [a], Marta Skaf [b], Asad-ur-Rehman Khan [c], Juan M. Manso [a]

[a] Department of Civil Engineering, Escuela Politécnica Superior, University of Burgos, c/ Villadiego s/n, 09001, Burgos, Spain
[b] Department of Construction, Escuela Politécnica Superior, University of Burgos, c/ Villadiego s/n, 09001, Burgos, Spain
[c] Department of Civil Engineering, NED University of Engineering and Technology, 75270, Karachi, Pakistan

ARTICLE INFO

Keywords:
Recycled aggregate self-compacting concrete
Ground granulated blast-furnace slag
Green aggregate powder
Stress-strain/load-deflection curve
Deformational-behavior prediction model

ABSTRACT

The high fine-aggregate content of Self-Compacting Concrete (SCC) means that its deformational behavior differs from that of vibrated concrete. SCC performance is further altered when industrial by-products are used as raw materials in those fractions. In this paper, the aim is to analyze and to model the deformational behavior under compression and bending of SCC containing 100% coarse and 0%, 50%, and 100% fine Recycled Aggregate (RA), limestone and RA green aggregate powders sized 0/0.5 mm, and Ground Granulated Blast-furnace Slag (GGBS) cement. After the fresh and mechanical characterization of the 18 SCC mixes that were produced, their compressive stress-strain and bending load-deflection curves were determined by continuously recording the applied load and the strain/deflection values of the SCC test specimens. 100% coarse RA yielded deformability levels in accordance with international standards, while higher fine RA contents increased deformation under compression and reduced it under flexural stress. SCC stiffness increased when GGBS was added, due to the adjustment of the proportion of cementitious matrix, while the use of limestone powder and, especially, RA powder had the opposite effect. Both compressive strain and flexural deflection were underestimated with existing theoretical models. However, the incorporation in the models of both exponential correction coefficients, dependent on the fine RA content, and partial adjustment coefficients, dependent on the types of cement and aggregate powder, produced optimal fits with the experimental stress-strain and load-deflection curves. In view of the deformational behavior, which was successfully modelled with maximum deviations of ±10%, fine RA may be used in combination with GGBS and limestone powder, although it is recommended that fine RA should not exceed proportions of 50%.

Abbreviations: ANalysis Of VAriance, (ANOVA); Ground Granulated Blast-furnace Slag, (GBBS); Natural Aggregate, (NA); Recycled Aggregate, (RA); Scanning Electron Microscope, (SEM); Self-Compacting Concrete, (SCC); water-to-cement, (w/c).

* Corresponding author. Department of Civil Engineering, Escuela Politécnica Superior, University of Burgos, c/ Villadiego s/n, 09001 Burgos, Spain.
E-mail addresses: vrevilla@ubu.es, vrevilla@ubu.es (V. Revilla-Cuesta), vortega@ubu.es (V. Ortega-López), mskaf@ubu.es (M. Skaf), asadkhan@neduet.edu.pk (A.-u.-R. Khan), jmmanso@ubu.es (J.M. Manso).

https://doi.org/10.1016/j.jobe.2022.104611
Received 14 March 2022; Received in revised form 21 April 2022; Accepted 2 May 2022
Available online 6 May 2022

1. Introduction

Concrete is the structural material *par excellence* of the construction sector [1]. Its reduced cost and versatile shapes explain why so many structures are built from this material [2]. Its remarkable behavior under compression and its strength, the main parameter for the design of structural elements, are virtually unrivalled [3]. Nevertheless, the deformability of concrete also needs to be considered [4–6]. On the one hand, the design under failure conditions of any concrete component requires knowledge of the longitudinal (load direction) stress-strain behavior under compression loads [7], which is defined according to the elastic and plastic zones of its stress-strain curve under compression [8,9]. On the other hand, the serviceability design of a concrete component requires a limit on its deflections [10]. For this purpose, determining the load-deflection curves of concrete under bending offers a more accurate approach to the concrete bending performance for serviceability [11].

Current regulations usually include simplified calculations to estimate the deformational behavior of concrete under both compression and bending [12,13]. However, the material considered for developing these models is a vibrated concrete produced with conventional materials, *i.e.*, Natural Aggregate (NA) and ordinary Portland cement [14]. This approach clashes with the increasing trend to incorporate alternative materials when producing concrete [15], mainly to increase its sustainability [16,17], which in turn modifies its deformational behavior [18].

As an example of this shift towards versatile and sustainable applications, Self-Compacting Concrete (SCC) can be mentioned. This type of concrete is characterized by its higher proportion of fine aggregate than vibrated concrete, which together with proper use of plasticizers, allows SCC to successfully fill the formwork without any external vibration [19]. It also reduces the carbon footprint of concrete by decreasing energy consumption during concreting [20]. Nevertheless, the use of a large amount of fine aggregate alters the proportion and composition of the cementitious matrix, which in turn increases plastic deformability (peak and fracture strains) [21,22]. Moreover, replacing the traditional limestone filler <0.063 mm with larger-sized powders, which usually produces a lower carbon footprint, due to their lower energy consumption during manufacturing [23], further alters the deformational behavior of SCC [24].

The use of sustainable aggregates produced from industrial by-products has also been gaining prominence in recent times, as it limits NA extraction from quarries [25]. One of the most widely used alternatives is Recycled Aggregate (RA), generally produced from precast crushed concrete components [26,27], that consists of NA and adhering mortar fragments (cementitious matrix). More deformable than NA [28], RA generates a weaker bond between the aggregate and the cementitious matrix [29,30]. Therefore, its use has the following effects on the deformational behavior of concrete:

- The addition of coarse RA instead of coarse NA leads to a decrease in the peak and the fracture strains of concrete under compression [31]. A phenomenon that is explained, because the use of this waste increases the likelihood of concrete cracking, leading to earlier plastic failure [32]. The treatment of coarse RA by reducing the content of adhered mortar or through carbonation improves its performance [33,34].
- The fine RA fraction has the opposite effect, as it appears to increase the plastic deformability of concrete [22]. The high content of mortar particles within this fraction, of lower stiffness than NA, explains these results [35].
- In relation to deflections under bending forces, the effect of both RA fractions depends on the characteristics of this material, such as the amount of adhered mortar or the strength of the parent concrete, and its adhesion to the cementitious matrix [36]. The higher deformability of RA should increase deflections, but early cracking decreases them [37,38].

Concrete sustainability is also promoted within the cement industry through the use of sustainable binders instead of conventional clinker, which allows reducing the carbon footprint of concrete [24]. The viability of various alternative binders has been analyzed in concrete production [39–41]. One of the most common is slag binder, *i.e.*, the partial replacement of conventional cement clinker with Ground Granulated Blast-furnace Slag (GGBS) [42]. This by-product from the steelmaking industry has binder properties and its use in cement manufacture is regulated in European standard EN 197–1 [43]. The use of GGBS in structural concrete has only recently been addressed in research and the study of its effect on the deformational behavior of concrete has basically been limited to the elastic regime [44]. Thus, it has been found that its use in the same proportion as Portland clinker increases elastic deformability and the plastic-strain levels [45]. Studies on the use of this alternative binder in the production of SCC are very scarce, although it appears that its addition in percentages up to 40% of binder weight can improve flowability, long-term strength, and plastic ductility in this type of concrete [22,46].

The simultaneous use of coarse RA and GGBS for the production of vibrated concrete has also been evaluated. According to the literature, the joint use of both by-products leads to a decrease in mechanical behavior, especially in splitting tensile and flexural strengths [47], while GGBS compensates for any worsening of durability that is a consequence of using coarse RA [48], resulting in an optimal substitution of 50% coarse RA and 40% GGBS [47]. The performance of concrete made with both by-products may be improved with the use of activating agents for GGBS such as lime [49] and desulfurization gypsum [50], which can at the same time reduce the carbon footprint of concrete by as much as 60% [51] and its costs by up to 23% [52]. Nevertheless, it must be noted that most of these studies refer to vibrated concrete, and only a few have addressed the specificities of SCC [53]. Furthermore, in all cases, mechanical and durability behavior of concrete is addressed in those studies, but not the simultaneous effect of both by-products on its deformational behavior, *i.e.*, on the stress-strain and load-deflection curves. A research gap that is bridged in this paper.

According to the above, the aim of this paper is to analyze the deformational behavior of an SCC containing full replacement of coarse NA with coarse RA; various percentages (0%, 50%, and 100%) of fine RA; replacement of ordinary Portland cement with CEM III/A, with 45% GGBS; and substitution of limestone filler with greener aggregate powders (limestone powder and RA powder, both 0/0.5 mm in size). The 18 sample mixtures were tested to obtain the stress-strain curves under compression and the load-deflection curves under bending, so that the effect and the interactions of the modifications on the composition of the mixtures could be

analyzed in detail. In addition, models obtained from existing prediction approaches are presented, which allow estimating this behavior and, therefore, approximating with greater accuracy the design of this type of concrete under failure and service conditions.

The study presented in this paper forms part of a broader research project that is intended to characterize highly sustainable SCC mixes in all their dimensions, at the same time as demonstrating the feasibility of their use. Some previously analyzed aspects are temporal fresh and mechanical-property behavior [54,55], the indirect estimation of their compressive strength [56], and the multi-criteria feasibility of their use [20]. In this study, the aim is to analyze deformational behavior under compression and bending in detail and to develop models with which to estimate this behavior. In this way, the authors consider that useful tools are provided for the successful design of structural elements with these types of concrete mixes.

2. Materials and methods

2.1. Raw materials

The components of the SCC mixes were cement, water, admixtures, and aggregates.

Two different types of cement as per EN 197–1 [43] were considered. On the one hand, CEM I 52.5 R (density of approximately 3.1 Mg/m^3) that is used for the development of concretes with optimum strength from a structural point of view [12,13]. On the other hand, CEM III/A 42.5 N (density around 3 Mg/m^3), a type of cement that has a GGBS content of around 45%, which increases its sustainability, approximately halving its carbon footprint [20].

Two different admixtures were added. First, a plasticizer to give the SCC adequate flowability. Second, a viscosity regulator, to reduce the amount of water required by the SCC to achieve high flowability.

Three aggregate fractions were used to prepare the SCC:

- Coarse aggregate 4/12.5 mm. All mixes incorporated this aggregate fraction of 100% RA to maximize SCC sustainability. This aggregate obtained from crushing and sieving defective precast concrete components rejected on quality grounds after their production. The structural purpose of the precast components meant that the characteristic compressive strength of the rejected components was around 45 MPa.
- Fine aggregate 0/4 mm. A combination of two fine aggregates, each of a different type, was incorporated in the SCC: rounded siliceous sand and recycled aggregate of the same origin as the coarse fraction.
- Aggregate powder. This fraction was the finest SCC aggregate needed to obtain adequate self-compactability [19]. First, limestone filler <0.063 mm was used, a product commonly utilized in the precast-concrete industry, which has a large carbon footprint because of the high consumption of energy during its manufacture [23]. Then, two greener aggregate powders, limestone and RA powders 0/0.5 mm in size, the latter of the same origin as the coarse and fine RA fractions, were also analyzed. Their larger particle size reduces energy consumption and, therefore, the carbon footprint, enabling the production of a more sustainable SCC [23], an aspect also favored by the recycled origin of the RA powder.

Table 1 details the density and the water absorption levels of all the aggregates, showing that the properties of both the NA and the RA had typical values [57]. The RA was therefore of lower density than the NA, although the RA had higher water absorption levels. Fig. 1 shows the granulometry curve of all aggregates, which in all cases was continuous and adequate for concrete production. A slightly higher content of fines was detected for the fine RA 0/4 mm than for the siliceous sand.

2.2. Mix design

For all the mix designs, the common objective was a class SF3, *i.e.*, a slump flow between 750 mm and 850 mm as per EN 206 [43]. First, the reference mix was designed following the indications of Eurocode 2 [13], seeking an optimal fit with the Fuller's curve, and performing field modifications to obtain the required slump flow. This mix incorporated CEM I, limestone filler <0.063 mm, 100% coarse RA, and 100% siliceous sand (0% fine RA). In addition, an effective water-to-cement (w/c) ratio equal to 0.50 was defined. Then, taking this mix as a reference, the rest of the alternative raw materials were progressively incorporated, applying volume correction for all component substitutions, thus obtaining the other SCC mixes of the study:

- First, two other mixes were designed with contents of fine RA of 50% and 100% (50% and 0% siliceous sand, respectively). The water content was adjusted so that the effective w/c ratio remained constant (value of 0.50).
- Subsequently, another three mixtures were proportioned with 0%, 50%, and 100% fine RA, although CEM I was replaced with CEM III/A. The coarse aggregate content was decreased by 20%, due to the higher grinding fineness of GGBS [53]. At the same time, the cement content was increased to compensate for the lower strength of GGBS compared to conventional cement clinker. In this way, homogeneous dragging of all aggregate particles was achieved without segregation, thus reaching an SCC of adequate strength with

Table 1
Water absorption and density of the aggregates.

	Limestone filler <0.063 mm	Limestone powder 0/0.5 mm	RA powder 0/0.5 mm	RA 0/4 mm	NA 0/4 mm	RA 4/12.5 mm
15-min water absorption (%)	0.37	1.95	6.32	5.77	0.18	4.90
24-h water absorption (%)	0.54	2.57	7.95	7.36	0.25	6.25
Density (Mg/m^3)	2.77	2.60	2.31	2.37	2.57	2.42

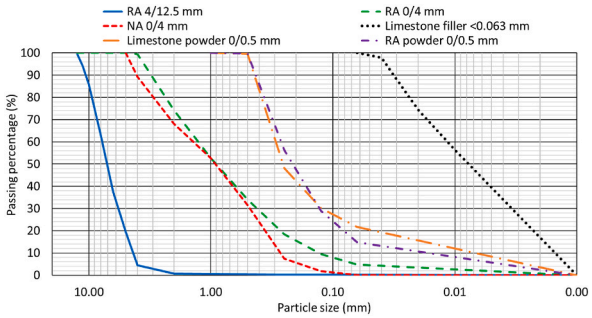

Fig. 1. Aggregate size gradation.

an SF3 slump-flow class. This increase in cement content in no way compromised the sustainability improvement of SCC. Considering the carbon footprints of CEM I and CEM III/A, at approximately 0.913 kg CO_2 eq/m^3 and 0.514 kg CO_2 eq/m^3, respectively [20,58], the cement-addition carbon footprints per cubic meter of SCC were 273.9 kg CO_2 eq/m^3 and 218.5 kg CO_2 eq/m^3, following the additions of CEM I and CEM III/A, respectively. Thus, the cement-addition carbon footprint decreased by around 20% when using CEM III/A. Finally, the water content was the same as for the mixes with CEM I and the same fine RA content, so the effective w/c ratio in these mixes was 0.40.

- Finally, another twelve SCC mixes were prepared, analogous to the previous ones, but where the limestone filler <0.063 mm was substituted by limestone powder (six SCC mixes) or RA powder (six other SCC mixes). It was necessary to increase the aggregate-powder content, due to the larger particle size (0/0.5 mm), to achieve an SF3 slump-flow class. The water content was accurately modified to maintain an effective w/c ratio of 0.50 for the CEM I mixes and 0.40 for the slag-cement SCC.

The study covered a total of 18 SCC mixes, whose composition in view of the above-mentioned aspects is shown in Table 2. The mixes were labelled with the code *BAP*, in which each letter represented one of the SCC components:

- *B*, cement type: *C* (CEM I) or *G* (45% GGBS, CEM III/A).
- *A*, aggregate powder: *L* (limestone powder), *F* (limestone filler), and *R* (RA powder).
- *P*, fine RA percentage: *0* (0% fine RA), *50* (50% fine RA), and *100* (100% fine RA).

2.3. Mixing procedure

A three-stage mixing process was implemented. The starting point was the non-simultaneous addition of aggregate and cement and a fractional addition of water, which maximized both cement hydration and aggregate water absorption [59]. This procedure resulted in an SCC of higher flowability, at all times achieving an SF3 slump-flow class. After several experimental trials, the three stages were, in detail:

- Incorporation of the aggregate and 50% of the mix water. Mixing for 3 min and resting for 2 min.
- Addition of CEM I or CEM III/A and the other half of the water. Mixing and resting for 3 and 2 min, respectively.
- Admixture pouring.

Table 2
Mix composition (kg/m^3).

Mix	CEM I # CEM III/A	Water	Limestone filler # Limestone powder # RA powder	Coarse RA	Siliceous sand # Fine RA
CF0	300 # 0	185	170 # 0 # 0	530	1120 # 0
CF50	300 # 0	210	170 # 0 # 0	530	560 # 510
CF100	300 # 0	235	170 # 0 # 0	530	0 # 1010
GF0	0 # 425	185	170 # 0 # 0	430	1120 # 0
GF50	0 # 425	210	170 # 0 # 0	430	560 # 510
GF100	0 # 425	235	170 # 0 # 0	430	0 # 1010
CL0	300 # 0	185	0 # 340 # 0	530	960 # 0
CL50	300 # 0	210	0 # 340 # 0	530	480 # 440
CL100	300 # 0	235	0 # 340 # 0	530	0 # 880
GL0	0 # 425	185	0 # 340 # 0	430	960 # 0
GL50	0 # 425	210	0 # 340 # 0	430	480 # 440
GL100	0 # 425	235	0 # 340 # 0	430	0 # 880
CR0	300 # 0	200	0 # 0 # 305	530	960 # 0
CR50	300 # 0	220	0 # 0 # 305	530	480 # 440
CR100	300 # 0	245	0 # 0 # 305	530	0 # 880
GR0	0 # 425	200	0 # 0 # 305	430	960 # 0
GR50	0 # 425	220	0 # 0 # 305	430	480 # 440
GR100	0 # 425	245	0 # 0 # 305	430	0 # 880

All mixes incorporated 4.50 kg/m^3 of plasticizer and 2.30 kg/m^3 of viscosity regulator.

2.4. Fresh- and hardened-state test methodology

Having manufactured the mixes, the slump-flow test was conducted as per EN 12350–8 [43], checking that all the mixes had a slump flow with a minimum value of 750 mm and a maximum value of 850 mm (slump-flow class SF3) according to EN 206 [43]. Later on, the specimens required for the tests performed in the hardened state were manufactured and stored for 28 days in a moist chamber at a humidity of 90 ± 5% and a temperature of 20 ± 2 °C, after which all the tests were conducted. The following tests were performed in the hardened state:

- Compressive strength (EN 12390–3 [43], two 10x20-cm cylindrical specimens), modulus of elasticity (EN 12390–13 [43], two 10x20-cm cylindrical specimens) and flexural strength (EN 12390–5 [43], two 7.5x7.5x27.5-cm prismatic specimens).
- Stress-strain behavior under compression (two 10x20-cm cylindrical specimens). A monotonic-load test was performed, with progressive loading at steps of 2 kN/s, in the same way as in the compressive-strength test, but continuously measuring the applied load and the strain within the concrete specimens. The setup for load and strain measurement is depicted in Fig. 2. Thus, the applied load (stress) was continually recorded through a load cell. Furthermore, three strain gauges were used to measure the longitudinal strain (in the load direction), although these strain measurements were complemented with 2 LVDTs that measured the displacement of the press (load) piston. The continuous recording of the load (stress) and strain yielded the stress-strain curves of the mixes under compression.
- Load-deflection curves under bending (two 7.5x7.5x27.5-cm prismatic specimens). A flexural-strength test was performed with the load applied at a rate of 2 kN/s, but with continuous recording of both the applied load and the deflection that the specimens underwent during the test. The test press recorded the measurements of both parameters on a continual basis.

2.5. Existing theoretical models for calculating the deformational behavior of concrete

There are different models to estimate the stress-strain behavior of concrete under compression. The most common practice is to estimate the peak and fracture strains of the stress-strain curve using fixed values. The US standard [12] specifies values of 2000 με for peak strain and 3000 με for fracture strain. The European Eurocode 2 [13] estimates these strains at 2000 με and at 3500 με, respectively. However, the model in the CEB-FIP model code [60] yields accurate predictions of the complete stress-strain curve of vibrated concrete containing conventional materials. This model [60] requires the calculation of two coefficients, firstly, coefficient K (Equation (1)), which depends on the modulus of elasticity (ME, in GPa) and the compressive strength (CS, in MPa) of the concrete, and, secondly, coefficient ε_0 (Equation (2)), which depends exclusively on the compressive strength. Once these coefficients are determined, the stress (σ, in MPa) corresponding to each strain (ε, in με) can be calculated through the compressive strength with Equation (3).

$$K = 1 + 2 \times e^{-\left(\frac{CS}{40}\right)} \tag{1}$$

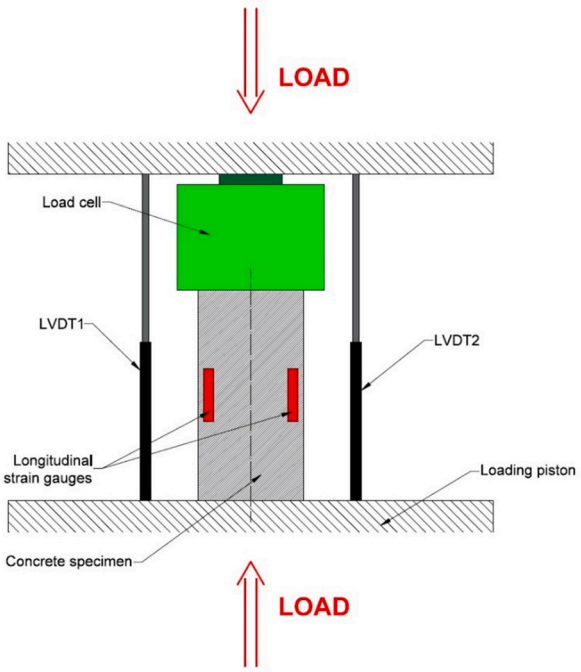

Fig. 2. Setup for recording the stress-strain curves under compression.

$$\varepsilon_0 = \left(4 + 3 \times K + \sqrt{(4 + 3 \times K)^2 - 40}\right) \times \frac{100 \times CS}{ME} \tag{2}$$

$$\sigma = \frac{CS \times \left(K \times \frac{\varepsilon}{\varepsilon_0} - \left(\frac{\varepsilon}{\varepsilon_0}\right)^2\right)}{1 + (K - 2) \times \frac{\varepsilon}{\varepsilon_0}} \tag{3}$$

The theoretical values of deflection in concrete can be obtained with the formulas to calculate deflections that are taken from the "Strength of Materials" theory [61]. The four-point flexural-strength test can be assimilated to a beam placed on a simple support with two equal loads that are symmetrically applied (Fig. 3). If the formula for the theoretical calculation of deflection in such a beam [61] is particularized for the specimen dimensions and its arrangement in this test (Fig. 3), an expression can be obtained that yields the theoretical deflection for each load that is applied during this test, and through which the theoretical load-deflection curve can be derived. This expression also has to account for the decreased inertia of the specimen section due to cracking, an aspect that is simulated by multiplying the theoretical deflection by a factor of ten [13]. In view of the above, the theoretical deflection in the central section of the specimen during the flexural-strength test (D, in mm) can be calculated with Equation (4), which is based on the modulus of elasticity of the concrete (ME, in kN/m^2) and the applied load (F, in kN).

$$D = 766666.7 \times \frac{F}{ME} \tag{4}$$

3. Results and discussion: fresh behavior and mechanical properties

This section provides an overview of the fresh and mechanical properties of the mixes for a proper characterization and understanding of their deformational behavior. A more detailed study of these properties can be found elsewhere [54,55].

3.1. Slump flow

All mixes had a filling-ability class SF3 as per EN 206 [43], as prescribed in the mix design. Each modification in the SCC composition affected slump flow in a different way, as shown in Fig. 4:

- 100% coarse RA was no impediment to high-flowability, due to the adequate coarse-to-fine-aggregate ratio in the SCC mix design, which compensated for the angular shape of the coarse RA [62].
- The slump flow increased with higher amounts of fine RA (Fig. 4a), although fine RA usually reduces the slump flow, due to its prolonged high water absorption and its irregular shape [63]. This situation is explained by the water compensation in the mix design and the higher fines content of fine RA compared to NA (Fig. 1), which augmented the cement-paste ratio.
- GGBS commonly tends to reduce SCC slump flow, because of its smaller particle size compared to conventional cement clinker [64], which in turn leads to more irregular dragging of the aggregate particles [53]. Nevertheless, in this research the proportions of coarse aggregate and cement paste were adjusted in the mix design when using GGBS, which led to an increased slump flow in the CEM III/A mixes (Fig. 4b). In this way, for the same fine RA content and type of aggregate powder, the use of CEM III/A increased the slump flow in most cases by around 30–60 mm.
- Each aggregate powder affected the slump flow of SCC (Fig. 4c) in different ways. On the one hand, the lowest slump flow values were obtained with RA powder 0/0.5 mm, because of its high water absorption levels and irregular shape [57]. On the other hand, limestone filler <0.063 mm gave the SCC a higher slump flow than limestone powder 0/0.5 mm of around 4–8%, due to its smaller particle size. The available literature shows that the slump flow can increase by up to 10%, if the precise amount of limestone filler is used, compared to the use of coarser limestone aggregate powders [65].

In addition, all mixes met the standard requirements (EN 206 [43]) of an SCC for viscosity (classes VS2 and VF2), passing ability (class PA1), and segregation resistance (class SR2), as detailed in another paper from the authors [54].

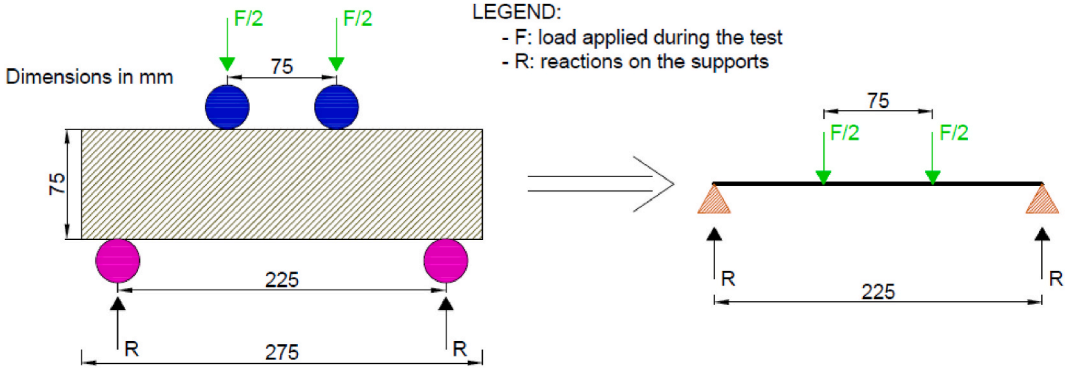

Fig. 3. Calculation of theoretical deflections.

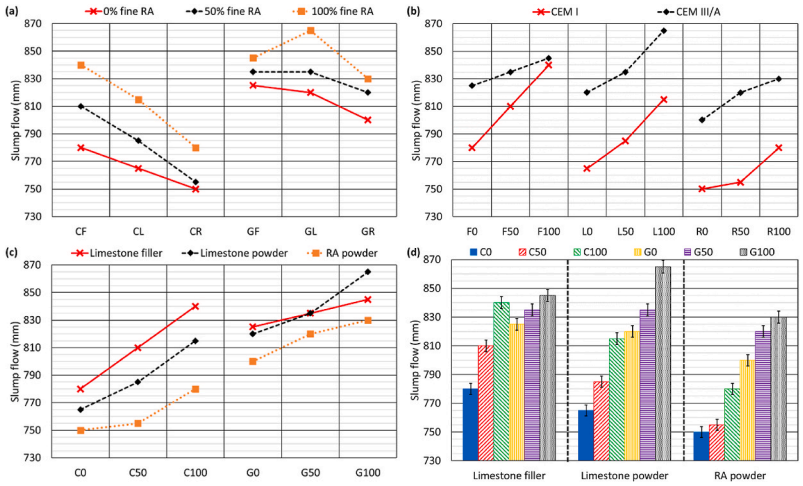

Fig. 4. Slump flow of SCC: (a) effect of the content of fine RA; (b) effect of cement type; (c) effect of the type of aggregate powder; (d) overview.

3.2. Mechanical properties: behavior under compression

The compressive strength and modulus of elasticity of the SCC mixes are shown in Fig. 5 and Fig. 6, respectively. It can be noted that the SCC with 100% coarse RA, 0% fine RA and limestone aggregate powders was adequate for structural use (around 45 MPa compressive strength and 40 GPa modulus of elasticity) [12,13], even though coarse RA usually reduces both concrete properties by around 20%, due to its higher flexibility and worse adhesion with the cementitious matrix than NA [8,66]. The addition of fine RA reduced both mechanical properties, due to the fact that fine RA usually increases the porosity of concrete, forming a cementitious matrix with poorer adherence to the coarse aggregate particles [35]. Weaker strength and increased porosity have also been reported when using coarse and fine RA simultaneously [67,68].

Conventional cement clinker is of higher strength and stiffness than GGBS [25]. Therefore, the use of that alternative binder usually reduces the modulus of elasticity and compressive strength of concrete in the short term [40], although modulus of elasticity values of up to 35 GPa can be achieved in the long term [46]. To compensate for this effect, as indicated in the mix design, the cement content of the SCC was increased when CEM III/A was used, so the expected reduction in the compressive strength and modulus of elasticity never occurred. Thus, moduli of elasticity of 40–45 GPa were achieved when this alternative binder was combined with 100% coarse RA, which were higher than the values found in the literature [46].

Finally, limestone filler (<0.063 mm) and limestone powder (0/0.5 mm) presented similar results in terms of compressive strength and modulus of elasticity, although limestone powder showed a slightly better performance. In some studies, the use of limestone aggregate powders has been shown to increase compressive strength by more than 10 MPa compared to other aggregate powders [65]. In this research, both limestone aggregate powders contributed to compressive strengths that were some 10–20 MPa higher than the strength achieved with RA powder 0/0.5 mm, because the most negative aspects of fine RA 0/4 mm were aggravated in its finer fractions [57], causing a large increase in concrete porosity and a significant decrease in the adhesion between the cementitious matrix and the aggregate particles [56].

3.3. Mechanical properties: behavior under bending

The flexural strength of each mix is shown in Fig. 7. It can be seen that the modifications to the mix composition had similar effects regarding the compressive strength and the modulus of elasticity:

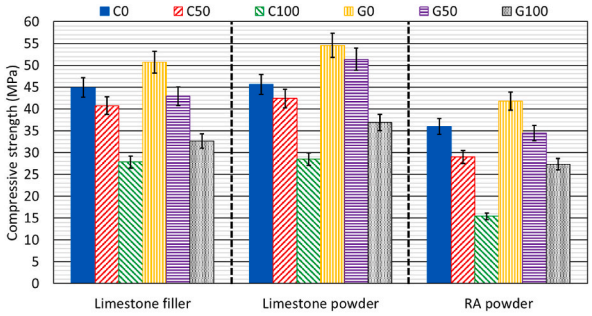

Fig. 5. 28-day compressive strength.

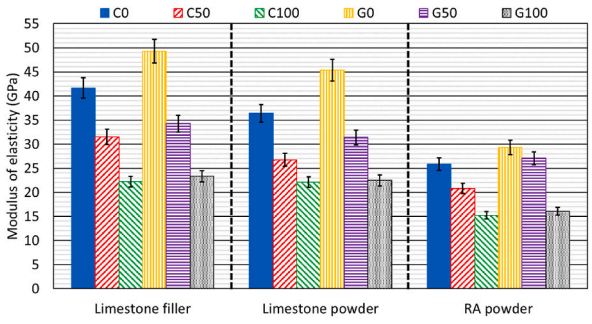

Fig. 6. 28-day modulus of elasticity.

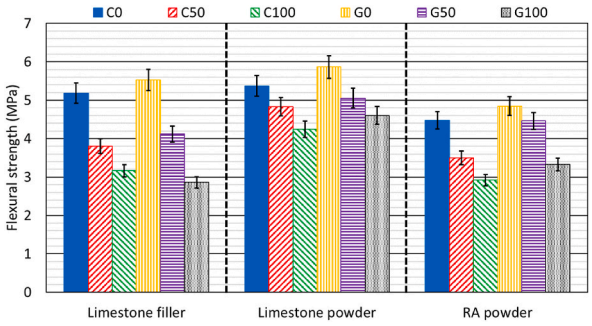

Fig. 7. 28-day flexural strength.

- The use of 100% coarse RA achieved flexural-strength values of around 5–6 MPa, adequate for structural concrete [12,13]. The quality of the coarse RA contributed to these strengths, as any dispersion of these aggregate properties can sometimes reduce flexural strengths to only 3–3.5 MPa [69]. Furthermore, the addition of CEM III/A also favored this aspect, as it improved the flexural strength of SCC, due to the increased cement content.
- Increasing the fine RA content reduced the flexural strength of the SCC, due to the reduced adhesion between the aggregate and the cementitious matrix [37]. Furthermore, these adhesion problems were generally amplified when fine RA was combined with coarse RA [38]. The combination of GGBS with 50% fine RA yielded a flexural strength of 4–5 MPa, 20% higher values than those obtained for vibrated concrete with this combination of by-products in other studies [47].
- Both limestone aggregate powders showed very similar performances that were better than the RA powder. The RA powder notably reduced the adhesion between the aggregate and the cementitious matrix, decreasing its tensile strength, which in turn reduced its flexural strength [19].

3.4. Microstructural analysis

Mix CR100 showed the worst mechanical properties. Images of the fragments obtained from the compressive-strength-test specimens were taken using a Scanning Electron Microscope (SEM), to analyze their behavior in detail. An image of the cementitious matrix

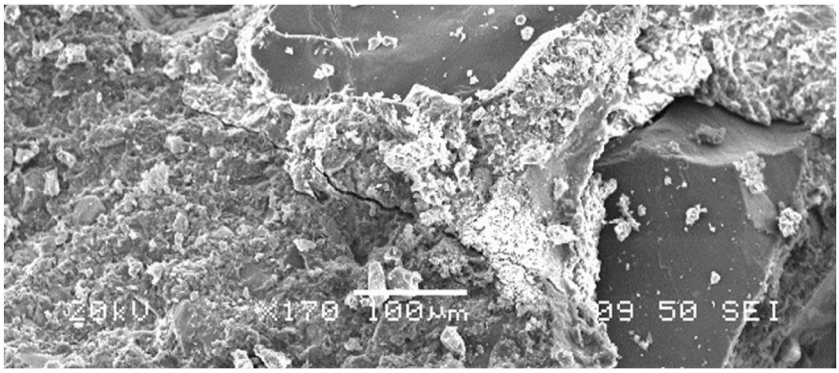

Fig. 8. SEM analysis of mix CR100.

and two particles of RA smaller than 1 mm are shown in Fig. 8: one at the top and the other to the right of the image. Detachment between the aggregate and the cementitious matrix was only observed in the particle located on the right-hand side. The decrease in mechanical properties was due not only to detachment phenomena, but also to a worsening of the quality of the cementitious matrix, possibly because of the high content of mortar particles and altered unhydrated cement in the fine RA and RA powder [57].

4. Results and discussion: stress-strain behavior under compression

4.1. Stress-strain curves: influence of mix composition

The stress-strain curves of the SCC mixes are shown in Fig. 9. All of them presented the usual form, an initially elastic zone and subsequently a zone of plastic deformation. Both the compressive strength and modulus of elasticity values were in line with those shown in section 3.2.

The plastic deformability of SCC is defined by the peak and fracture strains, *i.e.*, the strain at which the compressive strength is reached and the strain at which the final failure occurs, respectively [60]. These strains are shown in Fig. 10 (peak strain) and Fig. 11 (fracture strain):

- The addition of 100% coarse RA to an SCC containing ordinary Portland cement yielded peak and fracture strains in the range 2100–2700 με, close to the reference values indicated by the standards (Figs. 10a, 11a) and 2000 με for the peak strain and 3000 με for the fracture strain [12]. The strains values obtained were slightly higher than those found in vibrated concrete made with 100% coarse RA, which were found between 1800 and 2200 με [69], possibly due to the higher proportion of cement paste in the SCC. Therefore, the stress-strain behavior in the plastic regime containing large amounts of coarse RA meant that the SCC was suitable for structural use [12,13].
- Increasing the fine RA content enhanced the plastic deformability of the mixtures, so the addition of this RA fraction increased both the peak strain (Fig. 10a) and the fracture strain (Fig. 11a). An effect quite unlike the addition of coarse RA, which reduces both strains, due to the presence of mortar particles in the fine fraction of this alternative aggregate [34]. This increase of plastic deformability was higher when using CEM III/A, especially with regard to the peak strain. Thus, for example, the peak strain increased by 15% when adding 100% fine RA to an SCC manufactured with CEM I and limestone powder, while this increase was 21% when using CEM III/A.
- The mixes with CEM III/A had both lower peak and fracture strains (Figs. 10b and 11b), even though GGBS has a higher deformability than conventional cement [44]. The higher cement content compensated its higher deformability and even reduced the plastic strain of the G mixes, the peak strain never exceeded 3000 με in 8 of the 9 mixes, although in other studies the use of 20% GGBS had led to peak strains of 3000–3300 με [70]. In this way, when 45% GGBS was used as binder, 100% coarse RA and 50% fine RA were combined, peak and fracture strains close to the standard values (2000 με and 3000 με, respectively [12]) were obtained.

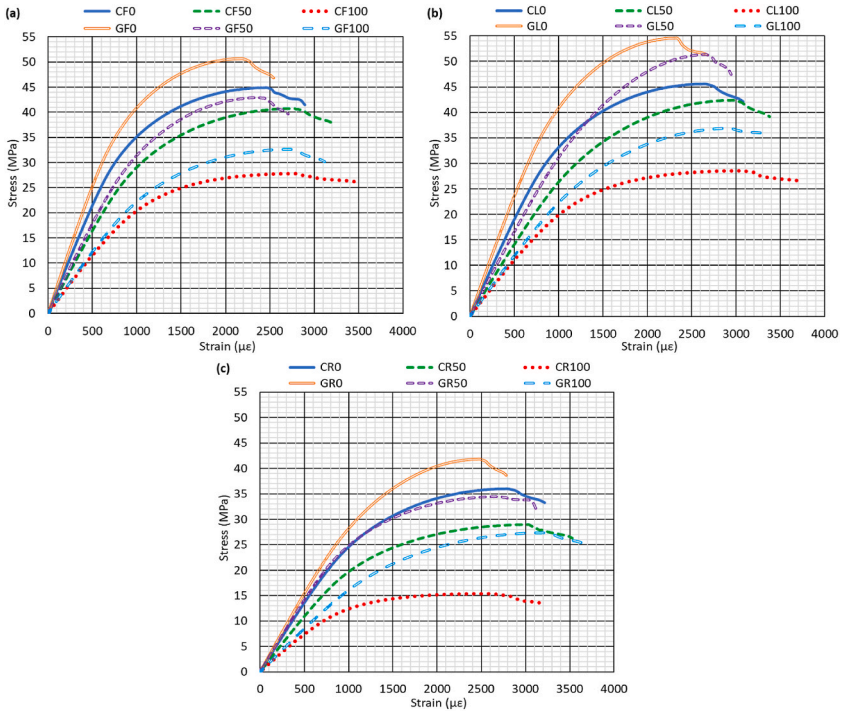

Fig. 9. Stress-strain curves: (a) mixes with limestone filler; (b) mixes with limestone powder; (c) mixes with RA powder.

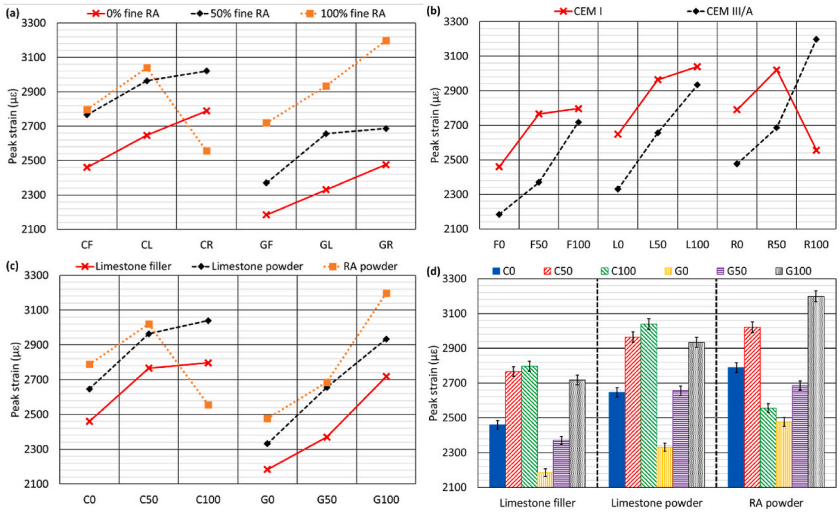

Fig. 10. Peak strain of the SCC mixes: (a) effect of fine RA content; (b) effect of cement type; (c) effect of aggregate powder type; (d) overview.

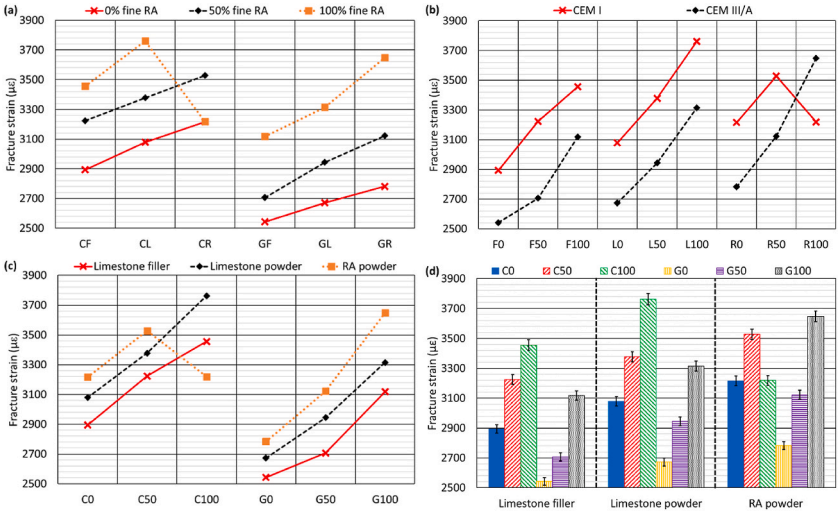

Fig. 11. Fracture strain of the SCC mixes: (a) effect of the content of fine RA; (b) effect of cement type; (c) effect of aggregate powder type; (d) overview.

- Both limestone aggregate powders demonstrated very similar behavior, although limestone filler slightly increased the stiffness in the plastic regime (Figs. 10c and 11c). Thus, the lowest peak strain was reached in mix GF0 (2196 με). The use of RA powder increased the plastic deformability of SCC, although not as noticeably as fine RA. In fact, mix CR100 showed peak and fracture strains of only 2556 με and 3216 με, respectively. A result that was explained due to the low compressive strength of this mix (15.4 MPa at 28 days), which caused its premature failure during the test [37].

The deformability of the SCC mixes conditioned another two aspects. On the one hand, the shape of the stress-strain curve. So, the mixes with CEM I, despite their lower strength, presented greater curvature than those containing CEM III/A (Fig. 9), because of their

Table 3
Three-way ANOVA ($\alpha = 0.05$) for stress-strain curves under compression.

		p-value (peak strain)	*p*-value (fracture strain)
Factors	**Fine RA content**	0.0000	0.0000
	Cement type	0.0000	0.0000
	Type of aggregate powder	0.0000	0.0000
Interactions	**Fine RA content and cement type**	0.0000	0.0049
	Fine RA content and type of aggregate powder	0.1822	0.1940
	Cement type and type of aggregate powder	0.0125	0.0108

higher plastic deformability. Nevertheless, the fracture strain was 1.1–1.25 times the peak strain in all the mixes, the highest values of this relationship were obtained in the most deformable ones (mixes C100). On the other hand, the deformability of the mixes also influenced their failure mode. It was noted that the compressive failure mode of the CEM I mixes with limestone aggregate powder and up to 50% fine RA was due to crushing, yielding the usual double inverted cone, as found in other studies [65]. The lower deformability of the mixes when CEM III/A was used (Figs. 10b and 11b) favored a more brittle failure of the SCC. On the contrary, the addition of 100% fine RA (Figs. 10a and 11a) and RA powder (Figs. 10c and 11c) increased the peak and fracture strains of SCC, which favored a more ductile failure, reflected by the appearance at failure of vertical cracks around the perimeter of the specimen, which was attributed to worse adhesion between the coarse RA and the cementitious matrix and the lower quality of the cementitious matrix [29].

Finally, Table 3 shows the three-way ANalysis Of VAriance (ANOVA) results for the peak and fracture strains, which were used to analyze whether the effect of each modification in the SCC composition was significant from a global approach. At a significance level of 0.05, it can be noted that every factor (fine RA content, cement type, and type of aggregate powder) had a significant effect on the plastic deformability of SCC. Furthermore, the interaction of the cement with both the fine RA content and the type of aggregate powder was significant, which indicates that the effect of increasing the fine RA content or modifying the aggregate powder type was different depending on the type of cement (CEM I or CEM III/A). Thus, for example, the increase in peak and fracture strains with the addition of 100% fine RA was greater when SCC incorporated CEM III/A. However, the effect of increasing the fine RA amount was the same regardless of the aggregate powder, *i.e.*, the interaction between these two factors was not significant.

4.2. Estimation of the stress-strain curves according to existing models

The stress-strain curve under compression of concrete can be fully estimated using the model in the CEB-FIP Model Code [60] that is detailed in section 2.5. To do so, all that is necessary is to know the compressive strength and modulus of elasticity of the concrete. As an example, Fig. 12 shows the comparison between the experimental stress-strain curves and those estimated through the aforementioned model for the SCC mixes containing limestone filler. In turn, Fig. 13 shows the quotient between the estimated and experimental strains for every load level in all the SCC mixes.

It can be noted that the model fit was especially accurate in the elastic zone (Fig. 12), in which the estimated and the experimental stress-strain curves practically coincided. However, in the plastic zone, both curves moved farther apart as the applied load increased, with the estimated stress-strain curves showing higher stiffness than the experimental curves within the plastic zone. The higher fines content of SCC compared to conventional vibrated concrete appears to lead to higher plastic deformation than expected from its modulus of elasticity and compressive strength [18]. This behavior was noted despite the addition of 100% coarse RA, which reduces the plastic deformability of concrete [31]. The increase in the content of fine RA improved the fit between both curves, so that its plastic deformability was more in accordance with the values of its compressive strength and modulus of elasticity. The type of cement in use appeared to have no significant influence on the fit of the model.

The aspects identified in Fig. 12 for the mixes containing limestone filler are confirmed in Fig. 13 for all the SCC mixes. The fit between the estimated and experimental stress-strain curves was correct in the elastic zone, with differences between the experimental and estimated strains of at most 10%, although the mixes with CEM I and 100% fine RA showed a higher underestimation up to 30% compressive strength in comparison with the other mixes. However, the strains were notably distant in the plastic zone, so that the estimated peak strain was 0.7–0.8 times the experimental one. The influence of the type of aggregate powder may also be noted, such that the underestimation of plastic deformability was higher when limestone aggregate powders were used. As with fine RA (Fig. 12), the mixes with RA powder appeared to have had a stress-strain behavior under compression that was more in accordance with the values of their compressive strength and modulus of elasticity.

4.3. Model adjustment for accurate estimation of stress-strain curves

As explained in the previous section, the fit of the CEB-FIP model (section 2.5) [60] with the experimental results of the mixtures was good within the elastic zone, but the fit within the plastic zone was defective. It was therefore decided to readapt this model for a proper estimation of the plastic behavior up to the peak strain, which entailed consideration of the following points:

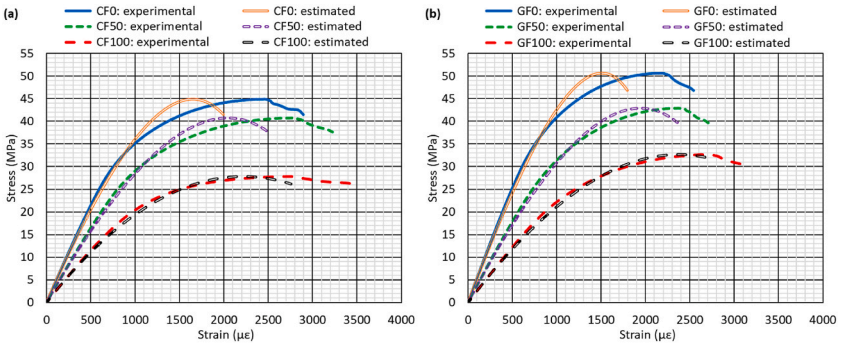

Fig. 12. Comparison between experimental stress-strain curves and stress-strain curves estimated with the CEB-FIP model [60] for mixes containing limestone filler: (a) CEM I; (b) CEM III/A.

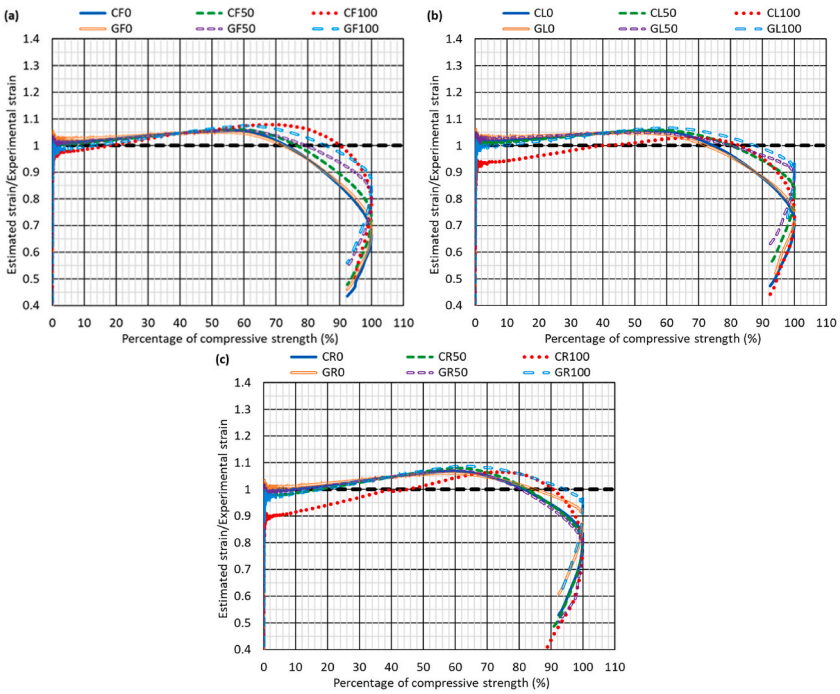

Fig. 13. Quotient between experimental compressive strain and compressive strain estimated with the CEB-FIP model [60]: (a) mixes with limestone filler; (b) mixes with limestone powder; (c) mixes with RA powder.

- An approach was performed to exclude the interactions between the factors (cement type, fine RA content, and type of aggregate powder) regarding the plastic behavior of SCC (Table 3).
- The model fit in the elastic zone was not modified, so the difference between the experimental and estimated strains continued to be at most ±10%. Efforts were focused on optimizing the fit in the plastic zone, to reduce the difference between both strains at most ±10%.
- A balance between the largest under- and overestimations of the experimental strain was sought, so that all of them were at most ±10%. The objective was to obtain an estimated stress-strain curve centered on the experimental one.
- The fracture zone of the stress-strain curves, *i.e.*, the zone of plastic behavior after the point of maximum stress, was omitted. The behavior in this zone was different for each mix and could not be generalized by readapting the CEB-FIP model [60]. Moreover, peak strain is the key parameter in structural design [12,13].

The proposed readjustment of the model involves calculating the coefficient K with Equation (1). Subsequently, once Equation (1) has yielded the value of coefficient K, the coefficient ε_0 may be calculated with Equation (2). These two aspects from the original model remain unchanged. The difference relates to the fact that the values of the coefficients K and ε_0 with which the stress-strain curve is calculated must be modified by a coefficient of an exponential nature (A and B, respectively), thus defining the coefficients K' and ε_0' (Equation (5) and Equation (6)). In addition, it is necessary to modify the strain, ε, which was multiplied by 1.05, in consideration of the effect of such high amounts of fines within an SCC. Thus, the formula of the stress-strain curve is shown in Equation (7).

$$K' = A \times K \tag{5}$$

$$\varepsilon_o' = B \times \varepsilon_0 \tag{6}$$

$$\sigma = \frac{CS \times \left(K' \times \frac{1.05 \times \varepsilon}{\varepsilon_0'} - \left(\frac{1.05 \times \varepsilon}{\varepsilon_0'} \right)^2 \right)}{1 + (K' - 2) \times \frac{1.05 \times \varepsilon}{\varepsilon_0'}} \tag{7}$$

Table 4
Values of the correction coefficient w.

Aggregate powder	Coefficient w
Limestone filler <0.063 mm	1.00
Limestone powder 0/0.5 mm	2.63
RA powder 0/0.5 mm	2.45

Coefficients A and B are calculated with Equation (8) and Equation (9), respectively, as a function of the fine RA content (FRA, in percent per one) and a correction coefficient, w, that depends on the type of aggregate powder. The values of the correction coefficient w are shown in Table 4. The values of coefficients A and B are independent of the type of cement (CEM III/A or CEM I).

$$A = w \times exp(0.40 - 0.27 \times FRA) \tag{8}$$

$$B = w \times exp(0.24 - 0.21 \times FRA) \tag{9}$$

This model presented an overall correlation coefficient R^2 of 96.8% and the stress-strain curves of the mixes showed an optimum fit, as may be seen in Fig. 14 for the mixes with limestone filler. Furthermore, it was successful at obtaining relative differences between all experimental and estimated strains below 10% in absolute value, as depicted in Fig. 15. It can therefore be stated that its use would be suitable for the estimation up to the peak point of the plastic stress-strain behavior under compression of the SCC mixes.

5. Results and discussion: load-deflection curves under bending

5.1. Load-deflection curves: influence of mix composition

Fig. 16 shows the load-deflection curves for all the SCC mixes. These curves showed a rising tendency, so much so that the deflection increment progressively decreased as the applied load increased. The most representative value of these curves was the maximum deflection, *i.e.*, the deflection at which the flexural strength was reached. The maximum deflection of each mix, as well as the effect of each factor (fine RA content, cement type and aggregate powder type) is shown in Fig. 17.

The use of 100% coarse RA yielded load/deflection ratios for the SCC mixes that were adequate for structural use [12,13]. For example, mixes CF0 and CL0 showed maximum deflections of 1.10 and 1.36 mm, respectively. The deflection levels were sufficient to guarantee proper design for serviceability [10].

The increase of the fine RA content reduced the flexural deformability of SCC (Fig. 17a), unlike the stress-strain behavior under compression. The addition of fine RA causes early concrete cracking when subjected to bending stresses [37], which leads to a very low increase in deflection from the initial cracking of the concrete to its failure, the point at which the flexural strength is reached [36]. This chain of events results in lower maximum deflections. A performance pattern that can be noted in Fig. 16, as the slope of the load-deflection curves was higher with increasing fine RA contents. Thus, for example, mixes CF0, CF50, and CF100 showed maximum deflections of 1.10 mm, 0.55 mm, and 0.39 mm, respectively.

The addition of large amounts of GGBS through the use of CEM III/A increased the flexural stiffness of SCC (Fig. 17b), the same trend as in the stress-strain behavior under compression. Deflection therefore decreased at same loading levels. Despite the lower stiffness of GGBS compared to Portland cement clinker [53], the increased cement content when using this alternative binder created an SCC with a higher volume of cementitious matrix that was, therefore, less ductile when bending. For example, the maximum deflections of mixes GF0 and GL0 were 0.74 mm and 0.82 mm, respectively, around 35% lower than those of the mixes containing CEM I, following similar trends that those found in the literature [17].

Finally, as with the stress-strain curves, limestone filler was the aggregate powder that provided greater stiffness to SCC, followed by limestone powder (Fig. 17c). The use of RA powder 0/0.5 mm increased the deflection range of SCC, unlike the effect of fine RA 0/4 mm. It therefore appears that the finer particles (<0.5 mm) of RA increased the flexural deformability of the SCC, while the addition of particles between 0.5 mm and 4 mm led to a loss of deformability, possibly due to decreased adhesion between the aggregate and the cementitious matrix [29].

As regarding peak and fracture strains, a three-way ANOVA (Table 5) showed that the effect of all the factors (fine RA content, cement type, and type of aggregate powder) was significant. No interaction of the aggregate powder with either the fine RA content or the cement type was detected, although there was significant interaction between the fine RA content and the cement type, which can be understood in two ways:

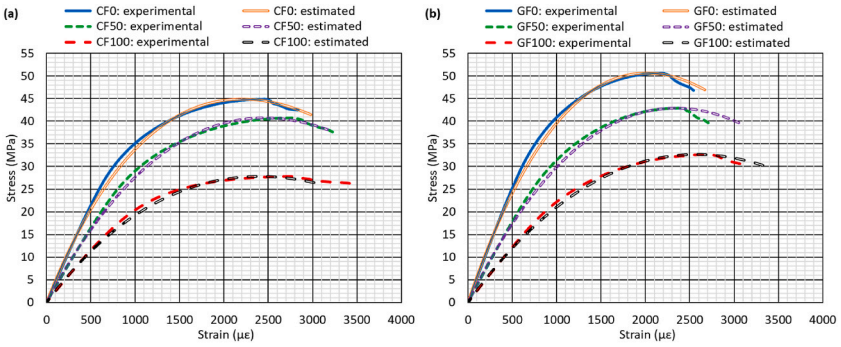

Fig. 14. Comparison between experimental stress-strain curves and stress-strain curves estimated with the developed model for mixes containing limestone filler: (a) CEM I; (b) CEM III/A.

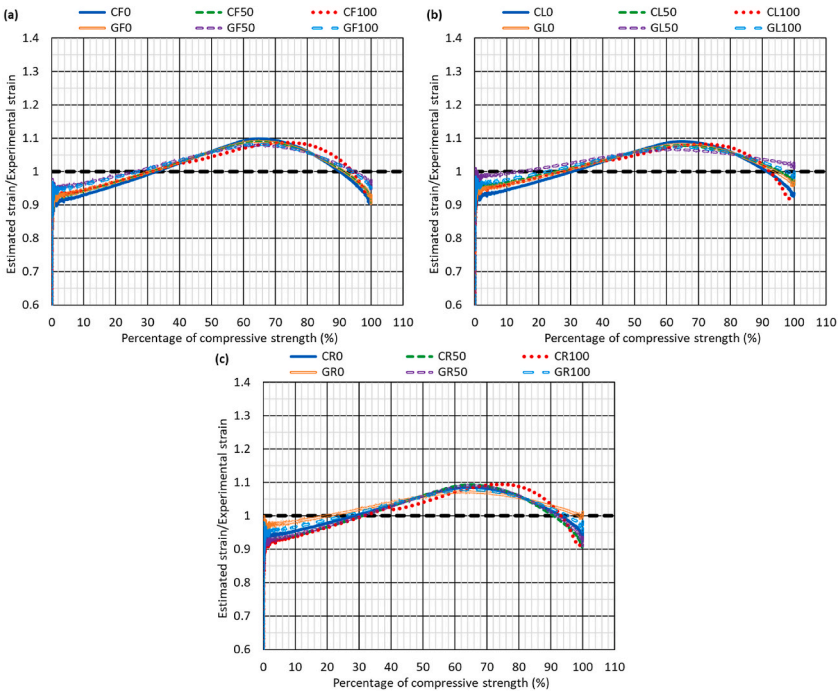

Fig. 15. Quotient between experimental strain and strain estimated with the developed model: (a) mixes with limestone filler; (b) mixes with limestone powder; (c) mixes with RA powder.

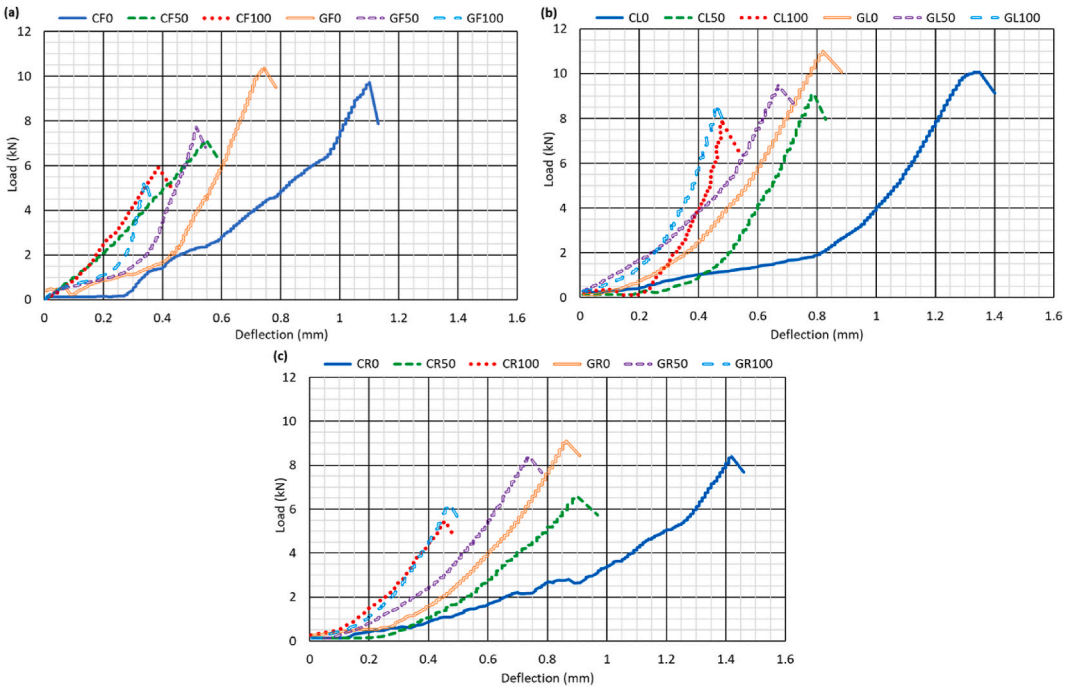

Fig. 16. Load-deflection curves: (a) mixes with limestone filler; (b) mixes with limestone powder; (c) mixes with RA powder.

- On the one hand, in the mixes with CEM I, the decrease in maximum deflection when adding 50% fine RA was approximately twice that of adding 100% fine RA (Fig. 17a). However, in the mixes with CEM III/A, this reduction was similar regardless of the amount of fine RA (50% or 100%).

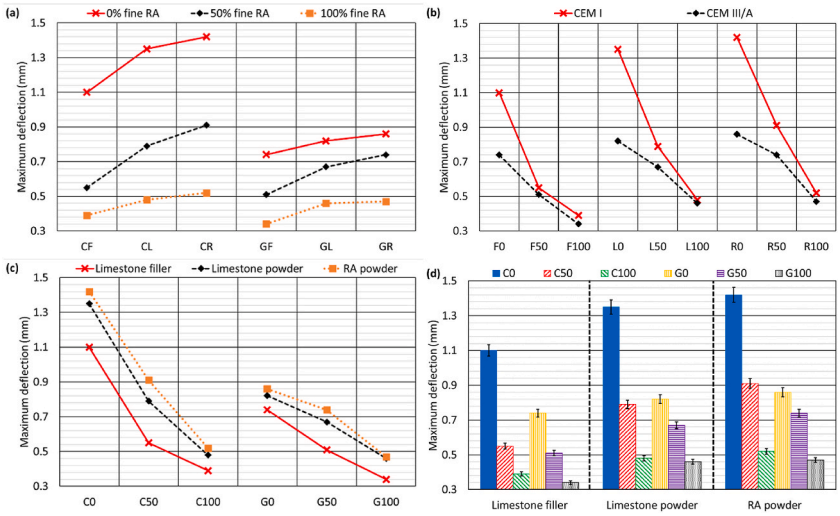

Fig. 17. Maximum deflection of the SCC mixes: (a) effect of the content of fine RA; (b) effect of cement type; (c) effect of the type of aggregate powder; (d) overview.

Table 5
Three-way ANOVA ($\alpha = 0.05$) for load-deflection curves under bending.

		p-value (maximum deflection)
Factors	**Fine RA content**	0.0000
	Cement type	0.0004
	Type of aggregate powder	0.0019
Interactions	**Fine RA content and cement type**	0.0015
	Fine RA content and type of aggregate powder	0.2554
	Cement type and type of aggregate powder	0.1766

- On the other, as shown in Fig. 17b, the mixes with 0% fine RA exhibited the largest loss of deformability when CEM I was replaced with GGBS, while the reduction in the maximum deflection was almost nil when the SCC contained 100% fine RA.

5.2. *Estimation of the load-deflection curves according to existing models*

The deflection that the concrete underwent can be estimated with Equation (4), shown in section 2.5. Fig. 18 shows the relationship between the deflection estimated with that formula and the experimental deflection (Fig. 16). It can be noted that at all times the

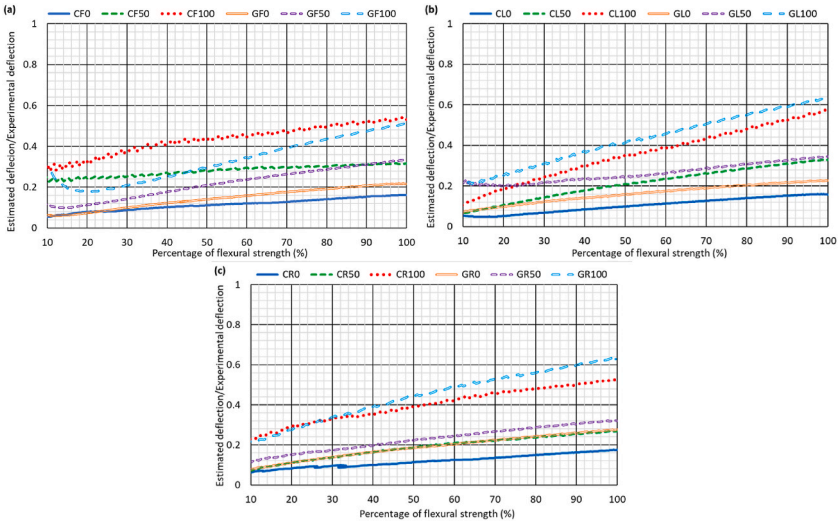

Fig. 18. Quotient between experimental flexural deflections and flexural deflections estimated with Equation (4): (a) mixes with limestone filler; (b) mixes with limestone powder; (c) mixes with RA powder.

estimated deflection was lower than the experimental one. This approximately linear relationship, especially as from 30% flexural strength onwards, showed a constant positive slope, so that the estimated deflection moved closer to the experimental one as the load increased. The patterns of this relationship were the same for all the SCC mixes, regardless of their composition, although the level at which the deflections were underestimated for each mix differed. Thus, the experimental deflections were less underestimated in the mixes with 100% fine RA, while the levels of underestimation for the other mixes were quite similar.

5.3. Model adjustment for accurate estimation of load-deflection curves

The load-deflection curves of the SCC mixes under study could not be correctly adjusted with the existing model (Equation (4)), so that the estimated deflection was at all times lower than the experimental one. Therefore, as with the stress-strain curves (section 4.3), the existing model was refined so that the estimation of the load-deflection curves could be properly performed. The aspects considered in this adjustment were as follows:

- A procedure for minimizing the influence of the interactions between the factors (Table 5) was developed. However, it was necessary to consider the influence of the cement type, in order to obtain adequate accuracy, unlike the stress-strain curves under compression.
- The maximum deviation between experimental and theoretical deflections was set at ±10%. The development of a model with that level of accuracy guarantees its applicability to structural design calculations [12,13].
- Finally, the adjustment was performed for flexural-stress values at and above 30% flexural strength. As indicated in section 5.2, there was no stabilization of the ratio between the estimated and experimental deflection up to that level of flexural stress. Therefore, the experimental deflections from the beginning of the test up to 30% flexural strength were ignored in the adjustment.

The idea behind the readjustment was to calculate the load-deflection curve using the existing model shown in Equation (4) (D, deflection in mm; F, load in kN; ME, modulus of elasticity in kN/m^2), but modifying the deflection values by a dimensionless coefficient C. The resulting model is shown in Equation (10).

$$D = C \times 766666.7 \times \frac{F}{ME} \tag{10}$$

Coefficient C is exponential in nature, as shown in Equation (11), and depends on two values. On the one hand, it depends on the applied force (F, in kN), which is the same as that introduced in Equation (10). This implies that the value of coefficient C will differ for each load value and, therefore, for each calculated deflection. On the other hand, the estimated bending failure load (F_f, in kN), characteristic of each SCC mix, must be also considered. In addition, it is necessary to define four adjustment coefficients: m, n, p_m, and p_n.

$$C = exp\left(p_m \times m - p_n \times n \times ln\left(\frac{F}{F_f}\right)\right) \tag{11}$$

The estimated failure load under bending (F_f, in kN) is determined by Equation (12), which depends on the compressive strength (CS, in MPa) of the SCC mix and two adjustment coefficients, a and b, the values of which are shown in Table 6. These two adjustment coefficients depend on the type of aggregate powder, so that the compressive strength accurately reflects the effects of both the fine RA content and the cement type on the failure load of the SCC under bending forces.

$$F_f = \frac{1.88}{a + b \times CS^2} \tag{12}$$

Coefficients m and n show the influence of the fine RA content and the cement type. These coefficients are not dependent on the type of aggregate powder and their values are shown in Table 7. Both coefficients are obtained using exponential formulas dependent on the percentage of fine RA (FRA, in percent per one).

The coefficients p_m (Table 8) and p_n (Table 9) depend on the type of aggregate powder and the cement type. However, the fine RA content (FRA, in percent per one) also has to be considered in some cases to improve the accuracy, especially with regard to the coefficient p_m.

The proposed model presented an overall coefficient R^2 of 92.6%, similar to the one obtained for the model of the stress-strain curves under compression. Thus, an optimal fit of the load-deflection curves was possible from the visual point of view, as shown in Fig. 19, for the mixes produced with limestone filler, in addition to an estimation of all deflection values with a maximum deviation of ±10%, as depicted in Fig. 20. The quotient between the estimated and experimental deflections showed no differences in the fit accuracy between the SCC mixes as a function of their composition, the more or less accurate fit depending on the individual values obtained during the test.

Table 6
Coefficients a and b for estimating the failure load under bending.

Aggregate powder	Coefficient a	Coefficient b
Limestone filler <0.063 mm	0.43	$-1.02{\cdot}10^{-4}$
Limestone powder 0/0.5 mm	0.26	$-3.10{\cdot}10^{-5}$
RA powder 0/0.5 mm	0.36	$-1.02{\cdot}10^{-4}$

Table 7
Coefficients m and n of the load-deflection-curve model.

Cement type	Coefficient m	Coefficient n
CEM I	$exp(0.66 - 1.07 \times FRA)$	$exp(-0.76 - 0.96 \times FRA)$
CEM III/A	$exp(0.33 - 0.85 \times FRA^2)$	$exp(-0.41 + 0.11 \times FRA)$

Table 8
Coefficients p_m of the load-deflection-curve model.

Type of aggregate powder	CEM I	CEM III/A
Limestone filler <0.063 mm	1.00	0.99
Limestone powder 0/0.5 mm	0.95	0.96
RA powder 0/0.5 mm	$0.88 + 1.21 \times FRA - 0.97 \times FRA^2$	$0.92 + 0.71 \times FRA - 0.90 \times FRA^2$

Table 9
Coefficients p_n of the load-deflection-curve model.

Type of aggregate powder	CEM I	CEM III/A
Limestone filler <0.063 mm	1.02	1.01
Limestone powder 0/0.5 mm	$exp(0.42 + 0.92 \times FRA)$	0.63
RA powder 0/0.5 mm	1.35	0.73

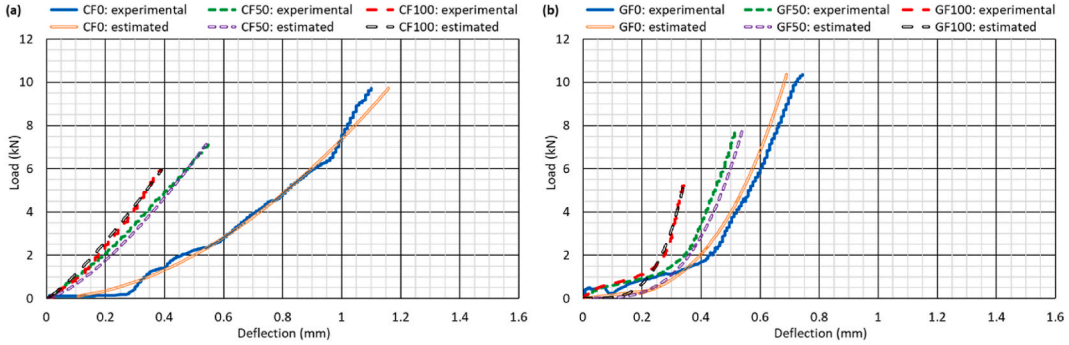

Fig. 19. Comparison between experimental load-deflection curves and estimated load-deflection curves with the developed model for mixes containing limestone filler: (a) CEM I; (b) CEM III/A.

6. Conclusions

In this paper, the deformational behavior of a Self-Compacting Concrete (SCC) of an SF3 slump-flow class has been evaluated. The SCC contained both coarse and fine Recycled Aggregate (RA), Ground Granulated Blast-furnace Slag (GGBS) cement, and aggregate powders with a lower carbon footprint than limestone filler, such as limestone and RA powders 0/0.5 mm. By continuously recording both the load and the strains/deflections in the compressive-strength and flexural-strength tests, it has been possible to obtain the stress-strain curves under compression and the load-deflection curves under bending, respectively, of the 18 SCC sample mixes. In this way, an analysis of every change in the composition of the SCC and its effect on its deformational performance could be conducted. Furthermore, existing models were refined for an accurate estimation of both curves. From those aspects under study, the following conclusions can be drawn:

- Adequate mix slump flows were achieved by adjusting the fines content when adding fine RA and the coarse-aggregate-to-cement-paste ratio when adding GGBS. These adjustments to the SCC composition also meant that the addition of 50% fine RA caused a decrease in the mechanical properties that was less than half the decrease due to 100% fine RA, and that the mechanical behavior improved when adding GGBS compared to the CEM I mixes performance. Finally, the SCC containing limestone powder 0/0.5 mm yielded the best in-fresh and mechanical performance.
- The use of 100% coarse RA yielded an SCC with adequate levels of both longitudinal strain in compression and deflection in bending. In fact, the values satisfied the requirements of international standards for structural use.
- The increased content of fine RA had opposite effects on the deformational behavior of the SCC. On the one hand, its high content of mortar particles caused a decrease in stiffness both in the elastic and plastic zone under compressive loading. Thus, both peak and fracture strains increased when using this waste. On the other, its reduced adhesion with the cementitious matrix led to earlier cracking of the SCC under bending, which resulted in decreased deflections at the same load level.

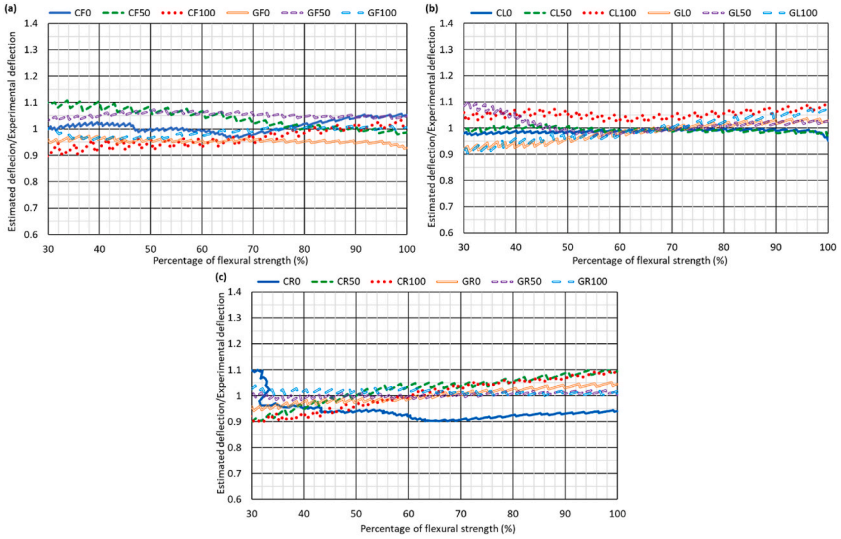

Fig. 20. Quotient between experimental deflection and estimated deflection with the developed model: (a) mixes with limestone filler; (b) mixes with limestone powder; (c) mixes with RA powder.

- Increasing the cement content and, therefore, the proportion of cementitious matrix when using a high GGBS content reduced the compressive and flexural stiffness of the SCC. Both the longitudinal strain under compression and the deflection under bending therefore decreased when using GGBS. An interaction between the amount of fine RA and the type of cement was detected, as the variation in the deformability of SCC following additions of RA was higher in mixes containing ordinary Portland cement.
- The use of limestone powder 0/0.5 mm instead of limestone filler slightly increased the deformability of the SCC under both types of stresses. The use of RA powder had the same effect as fine RA under compressive stress, as its use increased the peak and fracture strains. However, unlike fine RA, it also increased deflections in bending. Both green powders combined with GGBS further increased the deformability under compression of the SCC.
- The deformability of the SCC mixes under study was underestimated with the existing theoretical models for the prediction of the stress-strain curve under compression and the load-deflection curve under bending. Nevertheless, the use of correction coefficients of an exponential nature dependent on the amount of fine RA, as well as partial adjustment coefficients according to the type of cement and aggregate powder, refined those models and both curves could be adjusted with maximum deviations between the estimated and experimental values of $\pm 10\%$. The effect of the cement type could be avoided in the compressive behavior, while in the flexural behavior it had to be considered for an adequate adjustment.

To sum up, it can be affirmed that the simultaneous addition of coarse RA, GGBS, and limestone aggregate powders yielded an SCC with a deformational behavior suitable for structural use. The fine fraction of RA should be used more cautiously, due to its opposite effect under compressive and flexural stresses. It was not recommendable to add more than 50% fine RA to the SCC mix. The models developed in this study could be useful for assessing serviceability and failure conditions in the design of structural components with the designed SCC mixes, although the validity of any design calculations should at all times be carefully studied.

Authorship statement

Víctor Revilla-Cuesta: conceptualization, methodology, experimentation, formal analysis, data curation, writing-original draft, writing-review & editing.

Vanesa Ortega-López: conceptualization, supervision, writing-review & editing, project administration, funding acquisition.

Marta Skaf: conceptualization, methodology, supervision, writing-review & editing, funding acquisition.

Asad-ur-Rehman Khan: methodology, formal analysis, supervision, writing-review & editing, project administration.

Juan M. Manso: conceptualization, formal analysis, writing-review & editing, project administration, funding acquisition.

Declaration of competing interest

The authors declare that they have no known competing financial interests or personal relationships that could have appeared to influence the work reported in this paper.

Acknowledgements

The authors wish to express their gratitude for funding this research work to the Spanish Ministry of Universities, MICINN, AEI, EU, and ERDF [PID2020-113837RB-I00; 10.13039/501100011033; FPU17/03374]; the Junta de Castilla y León (Regional Government) and ERDF [UIC-231]; and the University of Burgos [SUCONS, Y135. GI].

References

[1] A.R. Khan, S. Fareed, M.S. Khan, Use of recycled concrete aggregates in structural concrete, Sustain. Constr. Mater. Technol. 2 (2019).
[2] F. Faleschini, P. Bragolusi, M.A. Zanini, P. Zampieri, C. Pellegrino, Experimental and numerical investigation on the cyclic behavior of RC beam column joints with EAF slag concrete, Eng. Struct. 152 (2017) 335–347, https://doi.org/10.1016/j.engstruct.2017.09.022.
[3] J.T. San-José, J.M. Manso, Fiber-reinforced polymer bars embedded in a resin concrete: study of both materials and their bond behavior, Polym. Compos. 27 (3) (2006) 315–322, https://doi.org/10.1002/pc.20188.
[4] D. Figueira, A. Ashour, G. Yıldırım, A. Aldemir, M. Şahmaran, Demountable connections of reinforced concrete structures: review and future developments, Structures 34 (2021) 3028–3039, https://doi.org/10.1016/j.istruc.2021.09.053.
[5] P. Anaya, J. Rodríguez, C. Andrade, B. Martín-Pérez, C.L. Hombrados, Determination of wires transfer length in prestressed concrete members with different levels of corrosion, Inf. Constr. 72 (558) (2020) 1–10, https://doi.org/10.3989/ic.71428.
[6] R. Lanti, M. Martínez, Biaxial bending and axial load in reinforced concrete sections, Numerical aproach, Inf. Constr. 72 (558) (2020) 1–9, https://doi.org/10.3989/ic.69148.
[7] P. Yuan, L. Xiao, X. Wang, G. Xu, Failure mechanism of corroded RC beams strengthened at shear and bending positions, Eng. Struct. 240 (2021), 112382, https://doi.org/10.1016/j.engstruct.2021.112382.
[8] R.V. Silva, J. De Brito, R.K. Dhir, Establishing a relationship between modulus of elasticity and compressive strength of recycled aggregate concrete, J. Clean. Prod. 112 (2016) 2171–2186, https://doi.org/10.1016/j.jclepro.2015.10.064.
[9] A. Memarzadeh, M. Nematzadeh, Axial compressive performance of steel reinforced fibrous concrete composite stub columns: experimental and theoretical study, Structures 34 (2021) 2455–2475, https://doi.org/10.1016/j.istruc.2021.08.130.
[10] X. Liang, S. Yin, Evaluation of the flexural behavior and serviceability of engineered cementitious composite-coral aggregate concrete beams reinforced with BFRP bars, Construct. Build. Mater. 308 (2021), 124937, https://doi.org/10.1016/j.conbuildmat.2021.124937.
[11] M. Rabi, K.A. Cashell, R. Shamass, Ultimate behaviour and serviceability analysis of stainless steel reinforced concrete beams, Eng. Struct. 248 (2021), 113259, https://doi.org/10.1016/j.engstruct.2021.113259.
[12] ACI-318-19, Building Code Requirements for Structural Concrete, American Concrete Institute (ACI). 38800 Country Club Drive, Farmington Hills, MI 48331, USA, 2019.
[13] Ec-2, Eurocode 2, Design of Concrete Structures. Part 1-1: General Rules and Rules for Buildings, CEN (European Committee for Standardization), 2010.
[14] J.J. Xu, W.G. Chen, C. Demartino, T.Y. Xie, Y. Yu, C.F. Fang, M. Xu, A Bayesian model updating approach applied to mechanical properties of recycled aggregate concrete under uniaxial or triaxial compression, Construct. Build. Mater. 301 (2021), 124274, https://doi.org/10.1016/j.conbuildmat.2021.124274.
[15] K.H. Mo, B.S. Thomas, S.P. Yap, F. Abutaha, C.G. Tan, Viability of agricultural wastes as substitute of natural aggregate in concrete: a review on the durability-related properties, J. Clean. Prod. 275 (2020), 123062, https://doi.org/10.1016/j.jclepro.2020.123062.
[16] S.N. Shah, K.H. Mo, S.P. Yap, J. Yang, T.C. Ling, Lightweight foamed concrete as a promising avenue for incorporating waste materials: a review, Resour. Conserv. Recycl. 164 (2021), 105103, https://doi.org/10.1016/j.resconrec.2020.105103.
[17] A. Santamaría, V. Ortega-López, M. Skaf, J.A. Chica, J.M. Manso, The study of properties and behavior of self compacting concrete containing Electric Arc Furnace Slag (EAFS) as aggregate, Ain Shams Eng. J. 11 (1) (2020) 231–243, https://doi.org/10.1016/j.asej.2019.10.001.
[18] F. Aslani, S. Nejadi, Mechanical characteristics of self-compacting concrete with and without fibres, Mag. Concr. Res. 65 (10) (2013) 608–622, https://doi.org/10.1680/macr.12.00153.
[19] S. Santos, P.R. da Silva, J. de Brito, Self-compacting concrete with recycled aggregates – a literature review, J. Build. Eng. 22 (2019) 349–371, https://doi.org/10.1016/j.jobe.2019.01.001.
[20] V. Revilla-Cuesta, M. Skaf, A.B. Espinosa, V. Ortega-López, Multi-criteria feasibility of real use of self-compacting concrete with sustainable aggregate, binder and powder, J. Clean. Prod. 325 (2021), 129327, https://doi.org/10.1016/j.jclepro.2021.129327.
[21] S.M. Mousavi Alizadeh, A. Rezaeian, I. Rasoolan, B. Tahmouresi, Compressive stress-strain model and residual strength of self-compacting concrete containing recycled ceramic aggregate after exposure to fire, J. Build. Eng. 38 (2021), 102206, https://doi.org/10.1016/j.jobe.2021.102206.
[22] V. Revilla-Cuesta, M. Skaf, A. Santamaría, V. Ortega-López, J.M. Manso, Assessment of longitudinal and transversal plastic behavior of recycled aggregate self-compacting concrete: a two-way study, Construct. Build. Mater. 292 (2021), 123426, https://doi.org/10.1016/j.conbuildmat.2021.123426.
[23] T.A. Rebello, R. Zulcão, J.L. Calmon, R.F. Gonçalves, Comparative life cycle assessment of ornamental stone processing waste recycling, sand, clay and limestone filler, Waste Manag. Res. 37 (2) (2019) 186–195, https://doi.org/10.1177/0734242X18819976.
[24] J. de Brito, R. Kurda, The past and future of sustainable concrete: a critical review and new strategies on cement-based materials, J. Clean. Prod. 281 (2021), 123558, https://doi.org/10.1016/j.jclepro.2020.123558.
[25] O. Gencel, O. Karadag, O.H. Oren, T. Bilir, Steel slag and its applications in cement and concrete technology: a review, Construct. Build. Mater. 283 (2021), 122783, https://doi.org/10.1016/j.conbuildmat.2021.122783.
[26] F. Fiol, C. Thomas, J.M. Manso, I. López, Transport mechanisms as indicators of the durability of precast recycled concrete, Construct. Build. Mater. 269 (2021), 121263, https://doi.org/10.1016/j.conbuildmat.2020.121263.
[27] M. Etxeberria, M. Konoiko, C. Garcia, M.Á. Perez, Water-washed fine and coarse recycled aggregates for real scale concretes production in barcelona, Sustainability 14 (2) (2022) 708, https://doi.org/10.3390/su14020708.
[28] Y. Mao, J. Liu, C. Shi, Autogenous shrinkage and drying shrinkage of recycled aggregate concrete: a review, J. Clean. Prod. 295 (2021), 126435, https://doi.org/10.1016/j.jclepro.2021.126435.
[29] V. Revilla-Cuesta, V. Ortega-López, M. Skaf, J.M. Manso, Effect of fine recycled concrete aggregate on the mechanical behavior of self-compacting concrete, Construct. Build. Mater. 263 (2020), 120671, https://doi.org/10.1016/j.conbuildmat.2020.120671.
[30] M. Bravo, A.P.C. Duarte, J.D. Brito, L. Evangelista, D. Pedro, On the development of a technical specification for the use of fine recycled aggregates from construction and demolition waste in concrete production, Materials 13 (19) (2020) 2619, https://doi.org/10.3390/MA13194228.
[31] C. Wang, J. Xiao, Evaluation of the stress-strain behavior of confined recycled aggregate concrete under monotonic dynamic loadings, Cement Concr. Compos. 87 (2018) 149–163, https://doi.org/10.1016/j.cemconcomp.2017.12.012.
[32] Z. Tang, W. Li, V.W.Y. Tam, Z. Luo, Investigation on dynamic mechanical properties of fly ash/slag-based geopolymeric recycled aggregate concrete, Compos. B Eng. 185 (2020), 107776, https://doi.org/10.1016/j.compositesb.2020.107776.
[33] V.W.Y. Tam, M. Soomro, A.C.J. Evangelista, Quality improvement of recycled concrete aggregate by removal of residual mortar: a comprehensive review of approaches adopted, Construct. Build. Mater. 288 (2021), 123066, https://doi.org/10.1016/j.conbuildmat.2021.123066.
[34] S. Luo, S. Ye, J. Xiao, J. Zheng, Y. Zhu, Carbonated recycled coarse aggregate and uniaxial compressive stress-strain relation of recycled aggregate concrete, Construct. Build. Mater. 188 (2018) 956–965, https://doi.org/10.1016/j.conbuildmat.2018.08.159.
[35] J. Sivamani, N.T. Renganathan, Effect of fine recycled aggregate on the strength and durability properties of concrete modified through two-stage mixing approach, Environ. Sci. Pollut. Res. (2021), https://doi.org/10.1007/s11356-021-14420-5.
[36] S. Yang, L. Li, Z. Sun, J. Wang, Q. Guo, Y. Yang, A closed-form fracture model to predict tensile strength and fracture toughness of alkali-activated slag and fly ash blended concrete made by sea sand and recycled coarse aggregate, Construct. Build. Mater. 300 (2021), 123976, https://doi.org/10.1016/j.conbuildmat.2021.123976.
[37] D. Gao, M. Lv, L. Yang, J. Tang, Flexural properties of high ductility cementitious composites with totally recycled fine aggregate, J. Mater. Res. Technol. 14 (2021) 1319–1332, https://doi.org/10.1016/j.jmrt.2021.07.047.
[38] M. Ghalehnovi, A. Karimipour, A. Anvari, J. de Brito, Flexural strength enhancement of recycled aggregate concrete beams with steel fibre-reinforced concrete jacket, Eng. Struct. 240 (2021), 112325, https://doi.org/10.1016/j.engstruct.2021.112325.
[39] O. Najm, H. El-Hassan, A. El-Dieb, Ladle slag characteristics and use in mortar and concrete: a comprehensive review, J. Clean. Prod. 288 (2021), 125584, https://doi.org/10.1016/j.jclepro.2020.125584.

[40] C.O. Nwankwo, G.O. Bamigboye, I.E.E. Davies, T.A. Michaels, High volume Portland cement replacement: a review, Construct. Build. Mater. 260 (2020), 120445, https://doi.org/10.1016/j.conbuildmat.2020.120445.
[41] M. Etxeberria, Evaluation of eco-efficient concretes produced with fly ash and uncarbonated recycled aggregates, Materials 14 (24) (2021) 7499, https://doi.org/10.3390/ma14247499.
[42] C.B. Cheah, L.E. Tan, M. Ramli, Recent advances in slag-based binder and chemical activators derived from industrial by-products – a review, Construct. Build. Mater. 272 (2021), 121657, https://doi.org/10.1016/j.conbuildmat.2020.121657.
[43] En-Euronorm, Rue de stassart, 36. Belgium-1050 Brussels, European Committee for Standardization.
[44] S.K. Sahoo, B.G. Mohapatra, S.K. Patro, P.K. Acharya, Evaluation of graded layer in ground granulated blast furnace slag based layered concrete, Construct. Build. Mater. 276 (2021), 122218, https://doi.org/10.1016/j.conbuildmat.2020.122218.
[45] R.R. Bellum, K. Muniraj, C.S.R. Indukuri, S.R.C. Madduru, Investigation on performance enhancement of fly ash-GGBFS based graphene geopolymer concrete, J. Build. Eng. 32 (2020), 101659, https://doi.org/10.1016/j.jobe.2020.101659.
[46] H. Zhao, W. Sun, X. Wu, B. Gao, The properties of the self-compacting concrete with fly ash and ground granulated blast furnace slag mineral admixtures, J. Clean. Prod. 95 (2015) 66–74, https://doi.org/10.1016/j.jclepro.2015.02.050.
[47] R.K. Majhi, A.N. Nayak, B.B. Mukharjee, Development of sustainable concrete using recycled coarse aggregate and ground granulated blast furnace slag, Construct. Build. Mater. 159 (2018) 417–430, https://doi.org/10.1016/j.conbuildmat.2017.10.118.
[48] R.K. Majhi, A.N. Nayak, Bond, Durability and microstructural characteristics of ground granulated blast furnace slag based recycled aggregate concrete, Construct. Build. Mater. 212 (2019) 578–595, https://doi.org/10.1016/j.conbuildmat.2019.04.017.
[49] R.K. Majhi, A.N. Nayak, B.B. Mukharjee, Characterization of lime activated recycled aggregate concrete with high-volume ground granulated blast furnace slag, Construct. Build. Mater. 259 (2020), https://doi.org/10.1016/j.conbuildmat.2020.119882, 119882.
[50] Y. Li, C. Qiao, W. Ni, Green concrete with ground granulated blast-furnace slag activated by desulfurization gypsum and electric arc furnace reducing slag, J. Clean. Prod. 269 (2020), 122212, https://doi.org/10.1016/j.jclepro.2020.122212.
[51] R.K. Majhi, A.N. Nayak, Production of sustainable concrete utilising high-volume blast furnace slag and recycled aggregate with lime activator, J. Clean. Prod. 255 (2020), https://doi.org/10.1016/j.jclepro.2020.120188, 120188.
[52] B.P. Lenka, R.K. Majhi, S. Singh, A.N. Nayak, Eco-friendly and cost-effective concrete utilizing high-volume blast furnace slag and demolition waste with lime, Eur. J. Environ. Civ. Eng. (2021), https://doi.org/10.1080/19648189.2021.1896581.
[53] O.K. Djelloul, B. Menadi, G. Wardeh, S. Kenai, Performance of self-compacting concrete made with coarse and fine recycled concrete aggregates and ground granulated blast-furnace slag, Adv. Concr. Constr. 6 (2) (2018) 103–121, https://doi.org/10.12989/acc.2018.6.2.103.
[54] V. Revilla-Cuesta, M. Skaf, A. Santamaría, J.J. Hernández-Bagaces, V. Ortega-López, Temporal flowability evolution of slag-based self-compacting concrete with recycled concrete aggregate, J. Clean. Prod. 299 (2021), 126890, https://doi.org/10.1016/j.jclepro.2021.126890.
[55] V. Revilla-Cuesta, F. Faleschini, C. Pellegrino, M. Skaf, V. Ortega-López, Simultaneous addition of slag binder, recycled concrete aggregate and sustainable powders to self-compacting concrete: a synergistic mechanical-property approach, J. Mater. Res. Technol. 18 (2022) 1886–1908, https://doi.org/10.1016/j.jmrt.2022.03.080.
[56] V. Revilla-Cuesta, M. Skaf, R. Serrano-López, V. Ortega-López, Models for compressive strength estimation through non-destructive testing of highly self-compacting concrete containing recycled concrete aggregate and slag-based binder, Construct. Build. Mater. 280 (2021), 122454, https://doi.org/10.1016/j.conbuildmat.2021.122454.
[57] F. Agrela, M. Sánchez De Juan, J. Ayuso, V.L. Geraldes, J.R. Jiménez, Limiting properties in the characterisation of mixed recycled aggregates for use in the manufacture of concrete, Construct. Build. Mater. 25 (10) (2011) 3950–3955, https://doi.org/10.1016/j.conbuildmat.2011.04.027.
[58] K.H. Yang, Y.B. Jung, M.S. Cho, S.H. Tae, Effect of supplementary cementitious materials on reduction of CO2 emissions from concrete, J. Clean. Prod. 103 (2015) 774–783, https://doi.org/10.1016/j.jclepro.2014.03.018.
[59] A.S. Brand, J.R. Roesler, A. Salas, Initial moisture and mixing effects on higher quality recycled coarse aggregate concrete, Construct. Build. Mater. 79 (2015) 83–89, https://doi.org/10.1016/j.conbuildmat.2015.01.047.
[60] Ceb-FIP, Model Code Volumes 1 and 2, 2012. Ch. du Barrage, Station 18 CH-1015 Lausanne, Switzerland.
[61] B. Dupen, Applied Strength of Materials for Engineering Technology, 10 ed., Purdue University, 2016. http://opus.ipfw.edu/mcetid_facpubs/48.
[62] I. González-Taboada, B. González-Fonteboa, J. Eiras-López, G. Rojo-López, Tools for the study of self-compacting recycled concrete fresh behaviour: workability and rheology, J. Clean. Prod. 156 (2017) 1–18, https://doi.org/10.1016/j.jclepro.2017.04.045.
[63] D. Carro-López, B. González-Fonteboa, J. De Brito, F. Martínez-Abella, I. González-Taboada, P. Silva, Study of the rheology of self-compacting concrete with fine recycled concrete aggregates, Construct. Build. Mater. 96 (2015) 491–501, https://doi.org/10.1016/j.conbuildmat.2015.08.091.
[64] V. Ortega-López, A. García-Llona, V. Revilla-Cuesta, A. Santamaría, J.T. San-José, Fiber-reinforcement and its effects on the mechanical properties of high-workability concretes manufactured with slag as aggregate and binder, J. Build. Eng. 43 (2021), 102548, https://doi.org/10.1016/j.jobe.2021.102548.
[65] F. Qu, W. Li, X. Zeng, Z. Luo, K. Wang, D. Sheng, Effect of microlimestone on properties of self-consolidating concrete with manufactured sand and mineral admixture, Front. Struct. Civ. Eng. 14 (6) (2020) 1545–1560, https://doi.org/10.1007/s11709-020-0678-4.
[66] B. Lei, W. Li, Z. Tang, F. Yang, Vertical bearing capacity of precast pier foundation filled with demolished concrete lumps, in: A. Kaboli, S. Shirowzhan (Eds.), Advances and Technologies in Building Construction and Structural Analysis, IntechOpen, 2020, https://doi.org/10.5772/intechopen.91205.
[67] B. González-Fonteboa, S. Seara-Paz, J. De Brito, I. González-Taboada, F. Martínez-Abella, R. Vasco-Silva, Recycled concrete with coarse recycled aggregate. An overview and analysis, Mater. Construcción 68 (330) (2018) e151, https://doi.org/10.3989/mc.2018.13317.
[68] R. Kurda, J. de Brito, J.D. Silvestre, A comparative study of the mechanical and life cycle assessment of high-content fly ash and recycled aggregates concrete, J. Build. Eng. 29 (2020), 101173, https://doi.org/10.1016/j.jobe.2020.101173.
[69] W. Li, B. Lei, Z. Luo, F. Yang, Construction technology of precast pier foundation filled with demolished concrete lumps, in: A. Kaboli, S. Shirowzhan (Eds.), Advances and Technologies in Building Construction and Structural Analysis, IntechOpen, 2019, https://doi.org/10.5772/intechopen.90091.
[70] G. Long, H. Liu, K. Ma, Y. Xie, W. Li, Development of high-performance self-compacting concrete applied as the filling layer of high-speed railway, J. Mater. Civ. Eng. 30 (2) (2018), 04017268, https://doi.org/10.1061/(ASCE)MT.1943-5533.0002129.